Design and Performance of Miniaturized Quarter-Wavelength Resonator Bandpass Filters With Attenuation Poles

H. Kanaya, *Member, IEEE*, K. Kawakami, F. Koga, Y. Kanda, and K. Yoshida

***Abstract*—For more size reduction of the high temperature superconducting coplanar waveguide (CPW) bandpass filter (BPF), we introduce the design method of the meanderline quarter-wavelength resonator BPF. The admittance and impedance inverters (J- and K-inverters) are realized by using interdigital gaps and meanderline short stubs. Also, we estimate the slope parameter of the meanderline resonator by using EM-simulator. In order to control the attenuation poles, we adjust the meanderline intervals and shapes of the cross-coupling section, so that we can design the frequency and number of the attenuation poles. The size of the 6-pole CPW quarter-wavelength resonator with two attenuation poles ($\mathrm{center\ frequency} = 2\ \mathrm{GHz}$) was 3.5 × 8 mm.**

***Index Terms*—Attenuation pole, bandpass filter, coplanar waveguide, meanderline, quarter-wavelength resonator.**

I. Introduction

In the wireless base station systems, which are used in the mobile and satellite telecommunication, high temperature superconducting (HTS) passive devices have an extremely high potential because of significant low insertion loss and high sensitivity. There are many reports on microstrip bandpass filter (BPF) [1]–[3], and HTS BPF based cryogenic receiver front-ends [4]. In order to reduce the cooling cost of the HTS filter subsystem, it is very important to miniaturize the HTS devices. The coplanar waveguide (CPW) structure is more advantageous than the microstrip structure because of only one side HTS coating and ease for size reduction.

In our previous studies [5]–[7], we designed the miniaturized cross-coupled CPW BPF by using highly packed meanderline half-wavelength ($\lambda/2$) resonators and interdigital gaps. In this paper, for further miniaturization, we designed and tested quarter wavelength ($\lambda/4$) resonator BPF by using interdigital gaps and meander-shape short stubs. Moreover, elliptic and quasielliptic filters using cross-coupled resonators have sharper skirt property than that of Chebyshev BPF in the same pole numbers [8]. So, we can design the $\lambda/4$ cross-coupled BPF with attenuation poles by controlling the meander shape of the resonators. The exact admittance (J)- and impedance (K)-inverters, and slope parameters of the $\lambda/4$ resonators are calculated by using the 2.5-dimensional electromagnetic field simulator (EM-simulator) (ADS; Agilent). The prototype YBCO miniaturized BPF ($\mathrm{center\ frequency} = 10\ \mathrm{GHz}$, 2-pole, $\mathrm{bandwidth} = 1\%$) was also tested in the cryogenic temperature.

Manuscript received October 4, 2004. This work was supported in part by the Grant-in-Aid for Encouragement of Young Scientists (B) from the Japan Society for the Promotion of Science (JSPS) and in part by a grant of Fukuoka project in the Cooperative Link of Unique Science and Technology for Economy Revitalization (CLUSTER) of Ministry of Education, Culture, Sports, Science and Technology (MEXT).

H. Kanaya, K. Kawakami, F. Koga, and K. Yoshida are with the Department of Electronics, Graduate School of Information Science and Electrical Engineering, Kyushu University, Fukuoka 812-8581, Japan (e-mail: kanaya@ed.kyushu-u.ac.jp).

Y. Kanda is with Department of Electronics, Faculty of Engineering, Fukuoka Institute of Technology, Fukuoka 811-0295, Japan.

Digital Object Identifier 10.1109/TASC.2005.850186

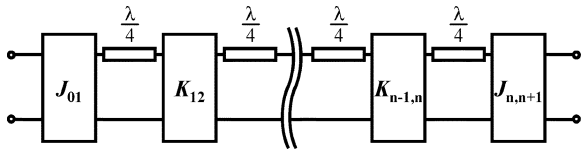

Fig. 1. Equivalent circuit model of the typical BPF with $\lambda/4$ resonators.

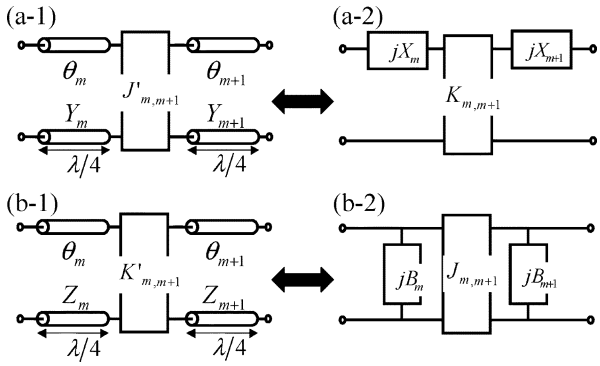

Fig. 2. Transmission-line based circuit model around the J-inverter (a-1) and equivalent circuit model (a-2), and those of the K-inverter (b-1) and equivalent circuit model (b-2).

II. Design of Chebyshev Quarter-Wavelength Resonator CPW Bandpass Filter

A. Measurement of the Slope Parameter

Fig. 1 shows the equivalent circuit model of the BPF with $\lambda/4$ resonators. The resonator is connected with the J- and K-inverters [9]. In order to realize the miniaturized BPF, these resonators are modified to the meanderline structures. So that, bending the resonators changes the slope parameters.

In order to design the J-inverter, the exact reactance slope parameter of the $\lambda/4$ resonator is measured and calculated. Fig. 2(a-1) shows the transmission-line based circuit model around the J-inverter ($J'_{\mathrm{m,m+1}}$). In the figure, θ_{m} and $\theta_{\mathrm{m+1}}$ are the electrical length of the transmission lines. Y_{m} and $Y_{\mathrm{m+1}}$

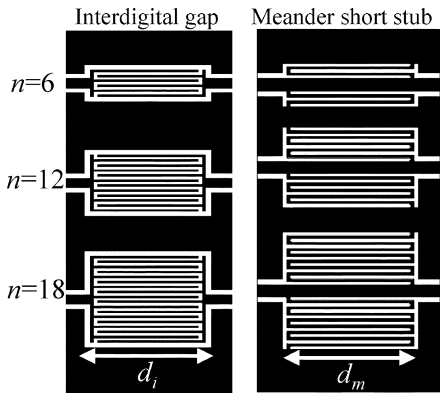

Fig. 3. Layout of the interdigital gap and meanderline short stub ($n = 6$, 12 and 18), respectively.

are the characteristic admittance of the transmission lines. The cascade matrix $[K]$ is given by

$$[K]=\begin{bmatrix} \frac{J'_{m,m+1}}{Y_m}\sin\theta_m\cos\theta_{m+1} & j\frac{J'_{m,m+1}}{Y_mY_{m+1}}\sin\theta_m\cos\theta_{m+1} \\ +\frac{Y_{m+1}}{J'_{m,m+1}}\cos\theta_m\sin\theta_{m+1} & -j\frac{1}{J'_{m,m+1}}\cos\theta_m\sin\theta_{m+1} \\ -jJ'_{m,m+1}\cos\theta_m\sin\theta_{m+1} & \frac{J'_{m,m+1}}{Y_{m+1}}\cos\theta_m\sin\theta_{m+1} \\ +j\frac{Y_mY_{m+1}}{J'_{m,m+1}}\sin\theta_m\cos\theta_{m+1} & +\frac{Y_m}{J'_{m,m+1}}\sin\theta_m\cos\theta_{m+1} \end{bmatrix}. \quad (1)$$

Near $\theta_i = \pi/2$ and $J'_{\mathrm{m,m+1}}/Y_i \ll 1$ (in case of week coupling), by substituting $J'_{\mathrm{m,m+1}} = K_{\mathrm{m,m+1}}Y_{\mathrm{m}}Y_{\mathrm{m+1}}$, $X_{\mathrm{m}} = -\cos\theta_{\mathrm{m}}/Y_{\mathrm{m}}$ and $X_{\mathrm{m+1}} = -\cos\theta_{\mathrm{m+1}}/Y_{\mathrm{m+1}}$ (where, X_{i} is the reactance of the resonator) in to (1), we obtain,

$$[K] = \begin{bmatrix} \frac{X_m}{K_{m,m+1}} & -jK_{m,m+1}+j\frac{X_mX_{m+1}}{K_{m,m+1}} \\ -j\frac{1}{K_{m,m+1}} & \frac{X_{m+1}}{K_{m,m+1}} \end{bmatrix}\times(-1) \quad (2)$$

Equation (2) is equal to that derived from the equivalent circuit model given in Fig. 2(a-2). We can replace the transmission-line based circuit model with equivalent circuit model. The reactance slope parameter (x_i) can be calculated as,

$$x_i = \frac{\omega_0}{2}\frac{\partial X_i}{\partial\omega}\bigg|_{\omega=\omega_0} = \frac{\pi}{4Y_i}. \quad (3)$$

In Fig. 2(b-1), Z_{m} and $Z_{\mathrm{m+1}}$ are the characteristic impedances of the transmission lines. In the figure, B_i is the susceptance of the resonator. The susceptance slope parameter (b_i) is measured in the same way as that of the x_i, and $bi = (\pi/4)Y_i$.

B. Realization of the J- and K-Inverter

Fig. 3 shows the layout of the J-inverter and K-inverter, respectively. They are realized by using interdigital gaps and meanderline short stubs. In the figure, n is the finger number and bending number of the inverters. Fig. 4 shows the EM-simulation results of the d_i and d_m dependence on both inverters. J/Y_0 and K/Z_0 are both saturated in large d_i and d_m regions. Fig. 5(a) and (5b) show the circuit model and layout of the J-inverter and K-inverter, respectively. In the figure, ϕ and β are the electrical length and phase constant of the transmission line, respectively. The exact J values and ϕ are calculated from the cascade matrix around the J-inverter section given in Fig. 5(a),

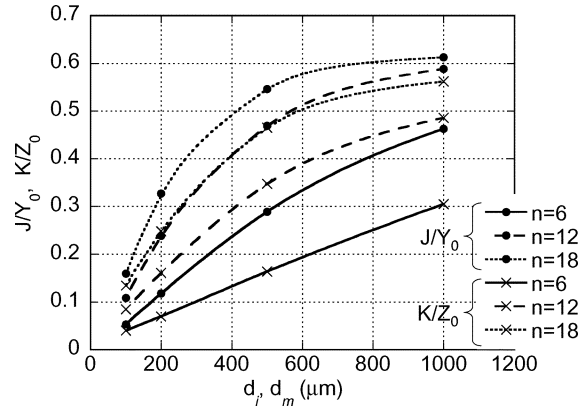

Fig. 4. EM-simulation results of the d_{i} and d_{m} dependences on inverters.

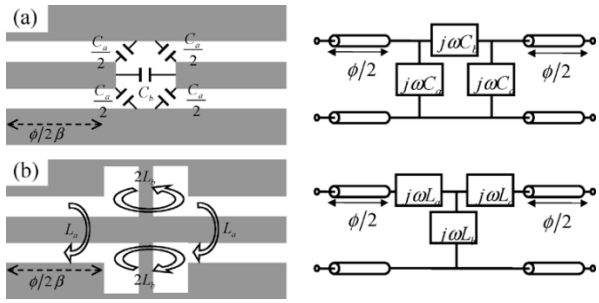

Fig. 5. Circuit model and layout of the J-inverter (a) and K-inverter, respectively.

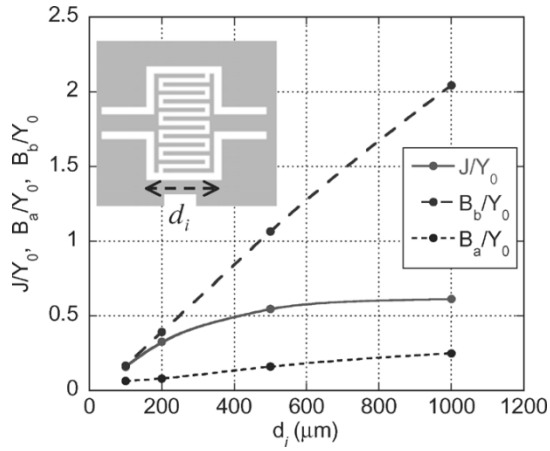

Fig. 6. Simulation results of the d_{i} dependence on B_{a}, B_{b} and J values, respectively ($n = 18$).

by using the EM simulator. The J value and ϕ are represented by the parameter B_{a} and B_{b}, and are given by,

$$\frac{J}{Y_0} = -Y_0\tan\left(\frac{\phi}{2}+\tan^{-1}\frac{B_a}{Y_0}\right), \quad (4)$$

$$\phi = -\tan^{-1}\left(\frac{2B_b}{Y_0}+\frac{B_a}{Y_0}\right)-\tan^{-1}\frac{B_a}{Y_0}. \quad (5)$$

Fig. 6 shows the EM-simulation results of the d_{i} dependence on B_{a}, B_{b} and J values, respectively, those are normalized by Y_0. B_b has a linear dependence on d_i. On the other hand, B_a is saturated in large d_i region, and J value is also saturated. In the case of K-inverter, L_a is also saturated in large d_m region.

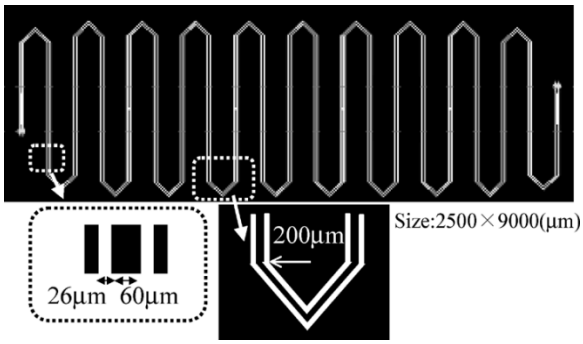

Fig. 7. Simulation layout of the 10-pole $\lambda/4$ CPW BPF.

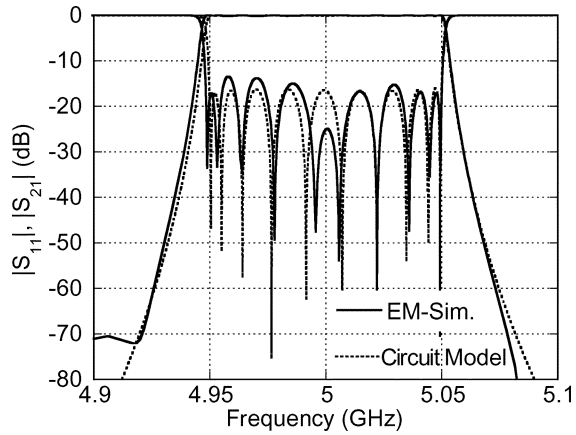

Fig. 8. Simulation results of the $n = 10\lambda/4$ CPW BPF.

When we design the BPF, which has wide bandwidth, it is expected that J and K value are saturated even if d_i and d_m becomes longer.

III. Design of CPW Quarter-Wavelength BPF

A. 5 GHz 10-Pole CPW Meanderline $\lambda/4$ BPF

Considering the b_i and x_i of the meanderline resonators, we design the standard Chebyshev CPW BPF by using the EM-simulator. The YBCO film is approximated as the perfect conductor and the thickness of the MgO ($\varepsilon_{\rm r} = 9.6$) substrate is 500 μm. The width of the signal line and gap interval is 60 μm and 26 μm (characteristic impedance $= 50\ \Omega$), respectively. Fig. 7 shows the simulation layout of the 10-pole $\lambda/4$ BPF ($f_0 = 10$ GHz, w $= 2\%$, ripple $(L_{\rm Ar}) = 0.1$ dB, meander radius $(r = 200\ \mu{\rm m})$. Where, the angular resolution dependence of the frequency response of the BPF is also discussed in the previous paper, so that this bending angle has almost the same properties as that of the smooth arc (r) [5]. In order to save the memory and CPU time during the simulation, we chose this bending angle. The filter size is 2.5 mm × 9 mm. Fig. 8 shows the simulation results of the 10-pole BPF. Simulated performance such as return loss in the passband and bandwidth are in good agreement with the circuit model.

B. 2 GHz 6-Pole CPW Meanderline $\lambda/4$ BPF With Attenuation Poles

In the previous paper, we introduced the design method of the CPW half wavelength meanderline BPF with attenuation poles

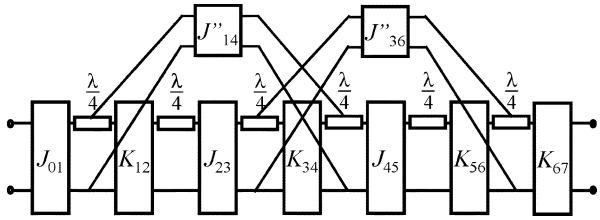

Fig. 9. Circuit model of the 6-pole $\lambda/4$ BPF with attenuation poles.

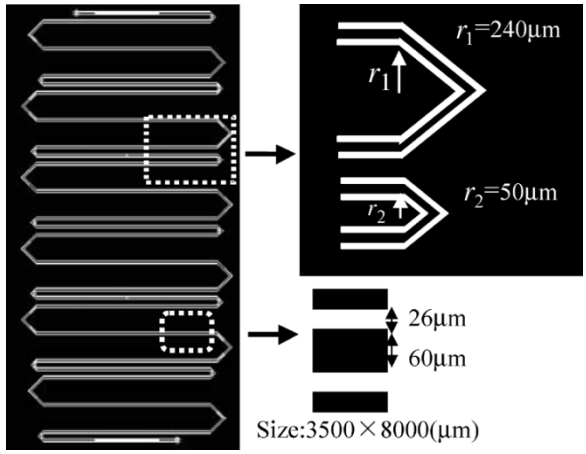

Fig. 10. Simulation layout of the 6-pole $\lambda/4$ BPF with attenuation poles.

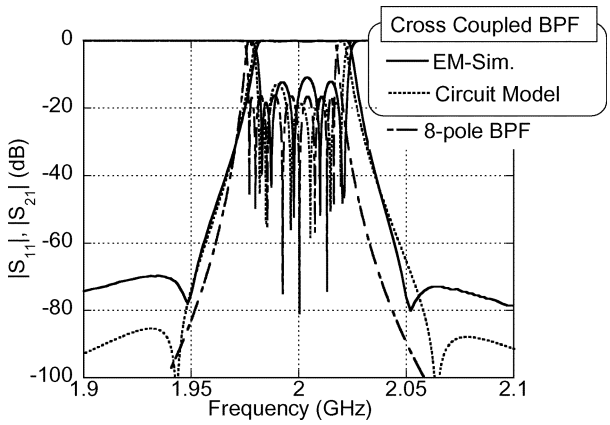

Fig. 11. Simulation results of the 6-pole $\lambda/4$ BPF with attenuation poles.

[7]. In this paper, we apply that method to $\lambda/4$ resonator BPF. By using the $\lambda/4$ resonator, we can expect that the filter size is reduced to half size. Figs. 9 and 10 show the equivalent circuit model and simulation layout of the 6-pole $\lambda/4$ BPF with two attenuation poles. The width of the signal line is 60 μm. The design parameters are $f_0 = 2$ GHz, $w = 2\%$, and $L_{\rm Ar} = 0.1$ dB, respectively. In order to fabricate the two attenuation poles at $\pm$50 MHz from center frequency, we decided the meander radius ($r_1 = 240\ \mu$m and $r_2 = 50$ mm) in the resonator. The filter size is 3.5 mm × 8 mm. Fig. 11 shows the simulation results and circuit model of the 6-pole $\lambda/4$ BPF with two attenuation poles. In the figure, the responses of the 8-pole Chebyshev BPF (no attenuation pole) are also plotted. This BPF has the same skirt characteristic of 8-pole standard Chebyshev BPF.

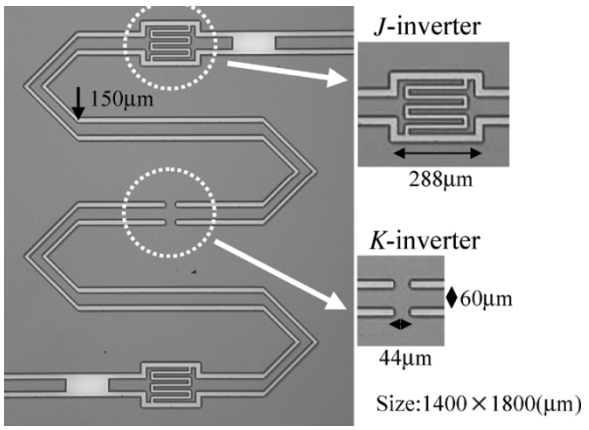

Fig. 12. Photograph of the prototype YBCO CPW $\lambda/4$ BPF for 10 GHz application.

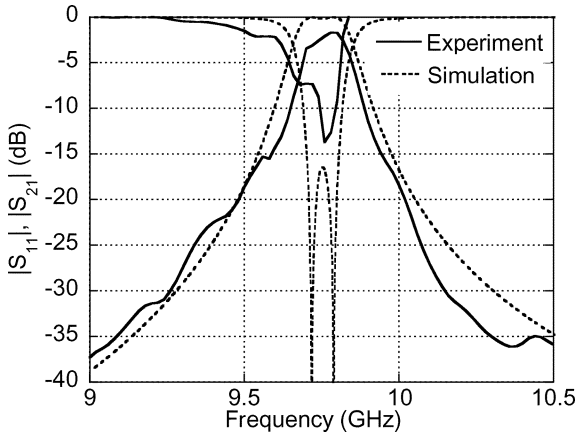

Fig. 13. Frequency responses of the 2-pole YBCO CPW $\lambda/4$ BPF at 20 K.

IV. Experimental Results of Prototype YBCO BPF

Fig. 12 shows the photograph of the prototype YBCO CPW $\lambda/4$ BPF for 10 GHz application. In the figure, the meander structure and interdigital gap are also printed. YBCO film used in this experiment was prepared on MgO single crystal, which has $\varepsilon_{\rm r} = 9.6$ and $\mathrm{thickness} = 500\ \mu\mathrm{m}$. The YBCO film thickness is 0.8 μm. This YBCO BPF has 2-pole and $\mathrm{bandwidth} = 1\%$, and filter size is 1.4×1.8 mm. The BPF was fabricated by the wet etching process. In the figure, we can see the over etching portion in the interdigital gap (J-inverter) and short stub (K-inverter). This BPF was placed in a vacuum chamber with refrigerator cooling system. We measured the S parameters by a vector network analyzer (HP8722C; HP) though the air coplanar probes (GSG-150; Cascade Microtech). Fig. 13 shows the frequency responses of the 2-pole YBCO CPW $\lambda/4$ BPF at 20 K. In the figure, broken lines show the S parameters of the EM simulation results. The bandwidth is similar to that of the circuit model. Because of the over etching portions, design ripple is not in full agreement with the simulation result in the pass band.

V. Conclusion

By measuring the exact J- and K-inverters, and slope parameter of the $\lambda/4$ resonators, we design the miniaturized quarter-wavelength resonator BPF. We can apply this design method to various pole number, center frequency and control of the attenuation poles. These design method is effective for reducing the cooling cost of the HTS filter subsystem. Moreover, in order to realize the RF-system LSI (System On a Chip), we will design and fabricate this miniaturized BPF on the CMOS chip.

References

[1] G. Tsuzuki, M. Suzuki, and N. Sakakibara, "Superconducting filter for IMT-2000 band," *IEEE. Trans. Microwave Theory Tech.*, vol. 48, pp. 2519–2525, Dec. 2000.

[2] J. S. Kwak, J. H. Lee, J. P. Hong, S. K. Han, W. S. Kim, and K. R. Char, "Narrow passband high-temperature superconducting filters of highly compact size for personal communication service applications," *IEEE Trans. Appl. Supercond.*, vol. 13, no. 1, pp. 17–19, Mar. 2003.

[3] W. Hattori, T. Yoshitake, and K. Takahashi, "An HTS 21-pole microstrip filter for IMT-2000 base stations with steep attenuation," *IEEE Trans. Appl. Supercond.*, vol. 11, no. 3, pp. 4091–4094, Sep. 2001.

[4] K. Satoh, T. Mimura, S. Narahashi, and T. Nojima, "Today and tomorrow of HTS technology applications," in *MWE Microwave Workshop Dig.*, 2000, pp. 102–117.

[5] H. Kanaya, T. Shinto, K. Yoshida, T. Uchiyama, and Z. Wang, "Miniaturized HTS coplanar waveguide bandpass filters with highly packed meanderlines," *IEEE Trans. Appl. Supercond.*, vol. 11, no. 1, pp. 481–484, Mar. 2001.

[6] H. Kanaya, Y. Koga, T. Shinto, and K. Yoshida, "Design and performance of miniaturized HTS coplanar waveguide bandpass filters with highly packed meanderlines," *IEICE Trans. Electron.*, vol. E58-C, no. 3, pp. 708–713, Mar. 2002.

[7] H. Kanaya, J. Fujiyama, R. Oba, and K. Yoshida, "Design method of miniaturized HTS coplanar waveguide bandpass filters using cross coupling," *IEEE Trans. Appl. Supercond.*, vol. 13, no. 2, pp. 265–268, Jun. 2003.

[8] J. S. Hong, J. J. Lancaster, D. Jedamzik, and R. B. Greed, "On the development of superconducting microstrip filters for mobile communications applications," *IEEE Trans. Microwave Theory Tech.*, vol. 47, no. 9, pp. 1656–1663, Sep. 1999.

[9] G. Matthaei, L. Young, and E. Jones, *Microwave Filters, Impedance-Matching Networks, and Coupling Structures*. New York: McGraw-Hill, 1964, pp. 427–440.